Trace metals in CO2-rich Green River Springs, Utah, USA: an analogue for engineered storage

Accepted Manuscript

Geological Society, London, Special Publications

Trace metals in CO_2-rich Green River Springs, Utah, USA: an analogue for engineered storage.

Mark Wilkinson, Kit Carruthers & R. Stuart Haszeldine

DOI: https://doi.org/10.1144/SP528-2022-69

To access the most recent version of this article, please click the DOI URL in the line above. When citing this article please include the above DOI.

Received 1 March 2022
Revised 8 June 2022
Accepted 27 June 2022

Supplementary material at https://doi.org/10.6084/m9.figshare.c.6150522

Trace metals in CO_2-rich Green River Springs, Utah, USA: an analogue for engineered storage.

Mark Wilkinson, Kit Carruthers, R. Stuart Haszeldine.

mark.wilkinson@ed.ac.uk

School of GeoSciences, Grant Institute, The King's Buildings, James Hutton Road, Edinburgh, EH9 3FE, UK

Abstract

Sedimentary rocks with high natural CO_2 concentrations provide invaluable analogues for the long-term engineered storage of CO_2. Some previous studies have reported high trace metal concentrations in sandstone aquifers exposed to CO_2, a cause for concern should stored CO_2 leak into underground sources of drinking water. However, the intensively studied Jurassic sandstone aquifer in the San Rafael – Green River (Utah, USA) area has trace metal concentrations that are within USA Environmental Protection Agency's limits for drinking water. Exceptions are As which is plausibly introduced into the aquifer by saline brines external to the aquifer, and salinity which largely is. This shows that CO_2 in aquifers does not inevitably cause trace metal contamination. CO_2-water-rock batch experiments elucidated the controls on the trace metal concentrations. After the addition of CO_2, the experiments reproduce well Cu, Cd, Hg, Ni and Zn, with less good agreement for Cr and Pb although these are still low compared to drinking water standards. Major cations used as fingerprints for mobilisation mechanisms suggest that the trace metals are largely derived by desorption, possibly from grain-coating Fe-oxides, rather than by the dissolution of mineral phases. Possible exceptions are Pb and Ni, plus As which is derived from saline brines.

Drinkable water is a valuable resource that must be protected in the event that CO_2 is stored underground below aquifers that are, or could be, used as underground sources of drinking water. Some published experiments have exposed samples of aquifer sandstones to CO_2-rich waters and have suggested that high levels of toxic metals may be released (e.g. Little and Jackson, 2010). Hence, here we present trace metal analyses of both natural porewaters and experimental brines to assess the trace-metal loads associated with CO_2 – rich porewaters on the Colorado Plateau, USA. The focus is on eight potentially toxic metals (As, Cd, Co, Cu, Hg, Ni, Pb, Zn) which are the subject of legislation within the European Union. Concentration limits for most of these metals are also set by the USA Environmental Protection Agency (EPA) though Ni and Zn are not subject to enforceable regulation (Environmental Protection Agency 2022A; Table 1). Zinc is listed in the EPA Secondary Drinking Water Standards (Environmental Protection Agency 2022B) due to it imparting a metallic taste to the water. However, these are guidelines to assist public water systems in managing their drinking water for aesthetic considerations and are not legally enforceable.

Two concentration levels are defined for each potential contaminant (Environmental Protection Agency 2022A). The Maximum Contaminant Level Goal (MCLG) is the level of a contaminant below which there is no known or expected risk to health. MCLGs allow for a margin of safety but are non-enforceable public health goals. Maximum Contaminant Level (MCL) is the highest level of a contaminant that is allowed in drinking water; MCLs are set as close to MCLGs as feasible using the best available treatment technology and taking cost into consideration. MCL's are legally enforceable standards in the USA. The secondary MCL (for Zn) is not legally enforceable. The salinity of the drinking water (expressed as total dissolved solids or TDS) is also regulated by the EPA as a secondary drinking water standard, with an upper limit of 500 ppm.

The area around the town of Green River on the Colorado Plateau in Utah, USA, has been extensively studied as an analogue for engineered CO_2 storage, as CO_2-rich springs and a cold-water 'geyser' (Crystal Geyser) are accessible. The regional hydrogeology is well described by Kampmann et al. (2009). The springs are largely sourced from the Navajo Sandstone which forms the regionally extensive Lower Jurassic 'N-aquifer' along with the Wingate Sandstone and Kayenta Formation (Kampmann et al., 2009). The aquifer is mostly supplied by meteoric water at outcrop in the San Rafael Swell (a broad anticline) to the west of the springs. Additionally, brine enters the aquifers via faults extending down to a Palaeozoic aquifer, formed by Lower Pennsylvanian and Mississippian limestone and dolomite formations (Hanshaw and Hill, 1969). Salinity in the brine is derived from the largely evaporitic Pennsylvanian Paradox Formation (Wilkinson et al., 2009). The erupted CO_2 is

mostly derived from crustal sources, with a 1–20% contribution from the mantle, with the CO_2 already mixed within the Paleozoic aquifer; Tenmile geyser is an exception with 16 to 99% mantle CO_2 (Wilkinson et al., 2009). Based on changes in pH, injection of CO_2 into the Jurassic aquifer occurs close to the Green River Airport Well and near Small Bubbling Spring (Kampmann et al., 2009). The Green River Airport well, sourced from exploration drill-hole Grand Fault 14–24, emits water from the Navajo Sandstone and is important as it is the spring closest to the recharge area of the aquifer (Kampman et al., 2014). It contains CO_2 but no detectable brine from deeper formations (Kampman et al., 2009). At Crystal Geyser, a well-studied cold water 'geyser', the majority of the water is derived from sandstones of the Jurassic Navajo (53 – 65%) and Entrada formations (45 – 33%), with only 1–2% Paradox brine based on major element geochemistry (Han et al., 2017) or approximately 10 % compared to approximately 10 – 20% for the other springs based on stable isotope analysis (Wilkinson et al., 2009). Previous work has concentrated on the geochemical evolution of the subsurface brines, especially Kampman et al. (2009, 2012, 2014), and the origin of the spring waters. This is not repeated here, where the mobilisation of potentially toxic trace metals is the main focus. The aim of the study is to determine which trace elements are mobilised by CO_2 in this area, and by extension in sites of engineered CO_2 storage, including any associated leakage. Both natural water samples and laboratory experiments are used to attempt to determine the source and controls on these elements. No analyses have been previously reported for most of the elements discussed here.

Methods

Field methods

As the Entrada, Wingate and Navajo sandstones are not exposed at the surface close to the sampled springs, they were sampled at the San Rafael Swell, located to the west-southwest of Green River. Here, the formations outcrop as the limbs on a large and spectacular anticline, before dipping eastwards into first a syncline and then a shallow anticline beneath the Green River springs. Four rock samples were collected at roadside locations adjacent to Interstate Route 70 from a cutting through the eastern limb of the San Rafael Swell, around 18 km west-southwest of Green River (Table 2 and Fig. 1). The stratigraphy of the sediments was worked out using the 1980 edition of the Geologic Map of Utah (1:500,000 scale) and accompanying sheet of representative stratigraphic columns and cross sections. Hammer samples of approximately 10 x 10 x 10 cm in size were taken. Sample S1 was chosen to include both a red/pink and white sandstone, and the boundary between them (Table 2). The sandstones at each location are relatively homogenous though Sample S3

included a thin (mm-scale) weathered 'crust' of red/pink sandstone, with an underlying white sandstone. Interactive maps with photographs of the outcrops are at https://goo.gl/wLpE1C.

Water Sample Collection

Figure 1 shows the location of the sampled springs. An interactive map with photographs is at https://goo.gl/a6D9un. Sampling of waters from 10 cold water springs was carried out on the 4 - 6th of October 2013. At each spring location, 8 separate water samples were collected and treated (Table 3). The sample containers, syringes and filters were pre-cleaned by the University of Texas (UT) using the following regime. Polypropylene bottles for cations and isotopes were rinsed with deionised (D.I.) water then soaked in micro-filtered water for 2 days; rinsed with D.I. water then soaked in 30% trace metal grade HNO_3 for 2 days; and finally rinsed in D.I. water then soaked in 18 MΩ D.I. water for 2 days before drying. Polypropylene bottles for anions, amber glass volatile organic analysis (VOA) vials and syringes were rinsed with D.I. then soaked in micro-filtered water for 2 days; rinsed with D.I. then soaked in 18 MΩ D.I. water for 2 days and then dried. Filters were rinsed with D.I. water then soaked in 18 MΩ D.I. water for 2 days. The sampling procedure for small (< 60 mL) bottles and vials was as follows: a full syringe of water was drawn from the geyser, as close to CO_2 bubbling as possible, then passed through the filter and discarded to the ground. This was repeated three times. The water was then passed through the filter into each sample container, rinsed and discarded three times; finally the water sample was passed through the filter to fill each sample container, leaving no headspace. Acids and reagents were added using a pipettor, to the volumes and concentrations in Table 3. The containers were sealed with a cap and Parafilm^{TM} before labelling.

For the batch experiments, water was collected in 1000 mL polypropylene bottles that were pre-cleaned with acid. If the geyser pool was large enough, the bottle was filled by submerging it and the fluid discarded to the ground three times, before filling to the brim and capping it a final time. The cap was sealed with Parafilm™. If the geyser was small, for example Little Bubbling Spring, then the bottle was filled to the brim using the syringe (unfiltered) instead of submerging it. The sampling for mercury (Hg) was carried out based on the method outlined in the UK Government Department for Energy and Climate Change (DECC) sampling guidance issued to North Sea oil and gas operators (Department of Energy & Climate Change, 2014). Samples were therefore collected in glass vials and preserved using 1M sulphuric acid and 1M potassium dichromate.

Spring water analysis

Major cations (Ca, K, Li, Mg, Na, NH_4^+) and anions (Br, Cl, F , NO_2^-, NO_3^-, PO_4^{-2}, SO_4^{2-}) of water samples were analysed on two Dionex ICS-1100 Ion Chromatography systems equipped with an AS-AP auto sampler at the Bureau of Economic Geology, University of Texas (UT) laboratories. Samples were diluted by a factor of 10 after collection, in order that Ca and SO_4^{2-} concentrations did not exceed 500 mg/L to conform with the limits of the analytical equipment. Repeat analysis of calibration standards (n = 4) gave the precision of the instrument, 1σ, as between 0.08% and 5.83% (median = 0.65%). Accuracy data was not provided by UT for the IC analysis. Major and trace cation data was obtained by Inductively Coupled Plasma Mass Spectroscopy (ICP-MS) for the 35 elements Ag, Al, As, B, Ba, Bi, Ca, Cd, Co, Cr, Cs, Cu, Fe, K, Li, Mg, Mn, Mo, Na, Ni, P, Pb, Rb, Sb, Se, Si, Sn, Sr, Th, Ti, Tl, U, V, Zn & Zr. Total dissolved solids (TDS) were calculated from the sum of these data. Mercury analysis was performed by Scientific Analysis Laboratories Ltd using Cold Vapour Atomic Fluorescence Spectroscopy (CV-AFS) in accordance with the recommended procedures of the UK Department of Energy & Climate Change (2014).

Spring water pH & alkalinity

The pH and alkalinities of spring waters were measured at 10 locations (Fig. 1). pH and temperature of the water in each spring was measured after sampling by dipping a combined portable pH and temperature probe into the geyser, connected to a Thermo Scientific Orion 3 Star pH meter, accurate to ± 0.01 pH and 0.1 °C, pre-calibrated at the University of Texas. After sample collection of 40mL samples, alkalinity was measured by adding 1.6N HNO_3 using a digital titrator and titrating to an endpoint pH of 4.50 ± 0.02. The starting pH, temperature and start and end readings on the titrator were entered into the USGS online alkalinity calculator using the fixed endpoint method (http://or.water.usgs.gov/alk/) for each sample. Temperatures were measured as close to the bubbling point of the spring as possible, therefore temperatures should reflect the upwelling water temperature, rather than stagnant water which could be affected by time-of-day and/or seasonal temperature variations.

Batch experiments

Pieces of sandstone were broken off the original field samples using a geological hammer, and these pieces reduced to chips with a jaw crusher. The chips were then disaggregated with a mortar and pestle, being careful not to grind the sample in order to preserve as best as possible any mineral overgrowths and to avoid exposing fresh mineral surfaces. Once disaggregated, 30 ± 0.1 g of sample was added to each flask in which the experiments were to be conducted, described by Wilkinson et al. (2020). The samples were allowed to react with 250 ± 1 mL of Crystal Geyser brine (Na 3270ppm;

Cl 3970 ppm) before CO_2 was added after approximately 3 months, then allowed to react for approximately another 3 months. The temperature was the ambient for the laboratory, approximately 21 °C; pH was measured more frequently within the first 10 days of the experiment and immediately following the start of CO_2 bubbling at day 82 than at other times, to ensure that rapid initial changes in pH were captured in the data.

Results

pH values for all spring locations lie in the range 6.3 - 6.8 (Table 4). The lowest pH values were measured at Green River Airport Well (pH 6.31) and Tenmile Geyser (pH 6.34). Alkalinity, measured as the concentration of bicarbonate, is also relatively constant across all the spring locations, with the obvious exception of Green River Airport Well again, which has an alkalinity of 2,335 mg/L, some 35% lower than the next lowest value of 3,589 mg/L at Tenmile Geyser. Water temperatures were also fairly constant, ranging from 13.8 - 18.5 °C, with the exceptions of Green River Airport Well (26.6 °C) and Side Seep (22.3 °C). The Side Seep location was stagnant water in a dried up creek, and measurements were taken mid-afternoon, therefore the elevated value of this location is probably not a reflection of the upwelling water temperature.

The spring waters are saline according to the classification of Kharaka and Hanor (2007; Table 5) with total dissolved solids (TDS) generally ranging from 11250 ± 44 mg/L (Crystal Geyser) to 17800 ± 65 mg/L (Torrey's Spring), with a median of 14900 mg/L. The exception is Green River Airport Spring which has a TDS of 3,750 ± 20 mg/L. Concentrations of As, Cu and Zn in Green River Airport Well are generally lower than other springs (Table 5). The remaining of the trace metals of interest (Cd, Cr, Hg & Pb) were not detected above analytical detection limits at any of the springs. Of the other 13 elements analysed (Table 5) Green River Airport Well has generally the lowest concentrations. A notable exception to this is Si which has a higher concentration (32 ± 3 mg / L) than any of the other springs by a factor of 8.

X-ray diffraction (XRD)

The Utah sandstones are dominated by quartz (57 to 90 wt % by XRD; Table 6). Gypsum, hematite and pyrite are below 1 wt. % (Table 6) and these values are indicative only of the probably presence of trace amounts of these minerals. The proportions of each are, however, quite similar across all of the samples. The Entrada formation sandstones are much more carbonate rich (12- 13 wt %) than the Wingate and Navajo sandstones (< 1 %). Most of the carbonate is calcite, dolomite and ankerite with only traces of siderite.

Batch Experiments

Initial pH values of the batch experiments are slightly higher than the field-measured pH for Crystal Geyser of 6.7 (Fig. 2 and Table S1), probably due to some CO_2 degassing during transport and storage of the samples collected 6 months prior to the start of the experiments. pH values then increase for all 4 batch reaction vessels in essentially the same manner to maximum values of between 8.8 (Entrada S1) and 9.0 (Wingate S3), recorded immediately after CO_2 bubbling commenced. There is then a rapid drop in pH for all samples after CO_2 bubbling begins to pH values of between 6.1 (Entrada S2) and 6.2 (Wingate S3). pH values then increase slightly for all the samples and maintain a steady mean pH of 6.4 for the remainder of the experiment (Fig. 2). These steady pH values are lower than at the start of the experiment, and therefore lower than the field-measured value at Crystal Geyser (although similar to the Green River Airport Spring and Tenmile Geyser field values; Table S1).

Trace metals in the batch experiments

The composition of the brines extracted from the batch experiments are given in Table S1. Concentrations of As and Cd were not detected above the analytical detection limits, with the exception of a single Cd data point for the Entrada S2 sample (Fig. 3). Concentrations of Cr, Hg and Pb are also low throughout duration of the experiment (Fig. 3). The addition of CO_2 at day 82 appears to mobilise some Cu, Hg, Pb and Zn (and possibly Cr), but these increased concentrations only persist for a maximum of approximately 30 days before returning to pre-CO_2 concentrations. Chromium concentrations for Entrada S1 reduce to lower than pre-CO_2 levels. Copper concentrations before CO_2 addition appear to be fairly constant and remain within the spring water range. Several days after CO_2 bubbling commences, spikes in concentrations occur for the Entrada S1 and Wingate S3 samples, with a maximum value of 49 ± 5 μg/L which is above the maximum spring value of 40 ± 3 μg/L (Torrey's Spring). However, concentrations then reduce back to lower than pre-CO_2 levels, and therefore within the range of the spring values. Concentrations of Ni are below detection limits for the majority of initial 3 months of the experiment, and therefore below the spring samples range of 4.4 ± 0.6 - 11.7 ± 0.9 μg/L, and remain so until day 97 where concentrations begin to increase for Navajo S4. Entrada S1 follows suit from day 112 and Entrada S2 and Wingate S3 from day 140. Final concentration values on day 166 are around the range of the natural spring waters (Fig. 3).

Zinc concentrations effectively remain constant throughout the experiment, with values at or exceeding the upper end of the springs' range of 6.7 ± 0.3 - 37 ± 7 μg/L (Fig. 3). The addition of CO_2 resulted in some spikes in concentrations for several days following, however final concentrations (20 ± 7 - 30 ± 10 μg/L) are slightly lower than starting concentrations (28 ± 9 - 38 ± 13 μg/L).

In summary, where concentrations exceed the limit of detection (LOD), concentrations of the trace metal are stable through the experiments, with essentially similar trends for the 4 rock samples. The addition of CO_2 to the flasks results in some temporary instability in concentrations of most of these elements, however concentrations stabilise again at similar, or lower, concentrations than pre-CO_2.The exception is Ni, where concentrations begin to rise from around 15 days after commencing CO_2 bubbling. Concentrations of Cu, Ni and Zn are comparable to those measured in the spring waters, while Cr, Hg and Pb were all mobilised to some extent during the experiments but not detected at all in the spring water samples. The exception is As, where the experiments do not mobilise the element above the limit of detection, despite the high concentrations (above legal drinking water standards) in the natural spring waters.

Major elements in the batch experiments

Concentrations of 8 major elements are presented here: Al, Ba, Ca, Fe, K, Mg, Mn & Sr (Fig. 4). For the most part, concentrations for these elements are very similar in each of the 4 batch samples with concentrations of 5 of these 8 elements falling into two distinct trends. Firstly, after a small initial rise, both K and Mg maintain constant concentrations up to the start of CO_2 bubbling, thereafter having a slight initial decrease (Fig. 4) but going on to slowly rise for the remainder of the experiment with bubbled CO_2. Concentrations of K remain largely within the range of the spring waters, although by the end of the experiment they have increased to slightly above. Magnesium concentrations for the batch experiments are consistently above the narrow range for the springs (Fig. 4).

Secondly, Ca, Mn and Sr show decreasing concentrations through the initial 3 months of the experiments for all samples. The minima are outwith the spring concentration range (Fig. 4). The addition of CO_2 to the flasks results in a rapid increase and then stabilisation of concentrations over a matter of days. The stabilised concentrations are within, or just below, the lower bounds of the spring concentrations.

Barium concentrations are initially within the range of spring concentrations for the first 3 months of the experiment, with the exception of Navajo S4 which initially increases in concentration to 71± 6 μg/L before returning to similar concentrations to the other samples by the end of this period. After CO_2 bubbling starts, there is a rapid increase in a matter of hours to maximum concentrations for all of the samples, with Navajo S4 again having the highest concentration of 140 ± 10 μg/L . This is a similar trend to Ca, Mn and Sr after CO_2 bubbling starts, however unlike these elements, concentrations of Ba then decline steadily over the next three months, possibly reaching stable

concentrations by the end of the experiment. With the exception of Navajo S4, the batch concentrations lie within the range of the spring values.

Of the remaining 3 elements, Fe does not appear to exhibit any systematic trend, although at the commencement of CO_2 bubbling, there are temporary slight increases in concentrations for Entrada S1 and Navajo S4, to values of 60 ± 20 μg/L and 110 ± 40 μg/L, respectively, followed by a general stabilisation and systematic increase in Fe concentration. Maximum batch Fe concentration values (180 ± 70 μg/L) are also significantly lower than the spring range of 1,190 - 20,600 μg/L. Finally, Al was detected at concentrations fluctuating between 140 ± 50 μg/L and 600 ± 200 μg/L prior to CO_2 bubbling, which is significantly higher than in the spring samples which are below the detection limit (BDL; 0.18 μg/L for ICP-MS). Concentrations then drop by a factor of 10 several days after CO_2 bubbling begins and remain at this level (or BDL) for the remainder of the experiment.

Discussion

Regionally, meteoric water enters the N-aquifer system in the San Rafael Swell and flows east, the first sampling point being the Green River Airport Well (Fig. 1). Although this well has high CO_2 levels, it has no detectable content of deep-sourced saline brine that ascend from the underlying Carboniferous strata (Kampmann et al., 2009), a relatively low salinity and low concentrations of Cu, Zn and As (Table 5). Hence, the N-aquifer has essentially 2 zones: from the outcrop in the San Rafael Swell to the first brine input after the Green River Airport Well, and beyond here. This model is supported by the behaviour of Cl-, a conservative tracer. A plot of Cl- vs Na+ shows that the springs lie close to a mixing line with the Ismay brine (Spangler, 1992) but with variable proportions of meteoric water and brine.

There is a general correlation between the distance along the aquifer flow-path beyond the Green River Airport Well and salinity (Fig. 5), suggesting that there are multiple points of entry for the brines into the N-aquifer, and not a single point of entry which would result in constant Cl- concentrations beyond the entry point, or even the 2 entry points identified by Kampmann (2009) as close to the Green River Airport Well and near Small Bubbling Spring. Using this porewater model, trace metals in the porewaters of the N-aquifer may hence be derived either from the Paradox brines, or from the N-aquifer rock matrix. There is evidence that at least some of the trace metal load in the aquifer waters is derived from the Paradox brines, although no analysis for this is known. The springs further down the flow path than the Airport Well all have higher salinity, a detectable content of brine from deep sources (1–2% in Crystal Geyser according to Han et al., 2017; 10 – 20% according to Wilkinson et al., 2009) and higher concentrations of As and Cu than the Airport Well

(Fig. 6). It is hence probable that the deep-sourced brines are introducing much of the As and Cu. Nickel concentrations in the Green River Airport Well are comparable to the other springs so there is no evidence that Ni is being significantly added by the deep brines (Fig. 6).

If the Paradox brines were of constant trace-element composition and no other processes were controlling trace metal concentrations, then there should be strong correlations between Cl and both As and Cu. For As, this is the case for 6 of the data points (Fig. 7) but 4 others have much lower As than would be predicted. This could indicate that some of the Paradox brines have low As concentrations, however there is no obvious spatial grouping of the low-As springs. However, As can be absorbed onto the aquifer rocks, see below where there is evidence that this is occurring in the batch experiments. The Cu data correlate well for all 8 out of 10 of the data points (Fig. 8). Torry's Spring and Little Bubbling Spring have higher than expected values but are not close spatially. The zinc data are too variable to discern any trend with distance and lack any obvious spatial pattern, again perhaps suggesting that the Paradox brines are of variable composition or that adsorption is affecting concentrations. The remaining trace metals (Cd, Cr, Hg, Pb) are BDL in all springs, so are either not present in significant concentrations in the deep brines or are present but are absorbed by the aquifer rock before the fluids arrive at the springs. Given the lack of spatial correlation between wells that do not fit the simple two-fluid mixing model, then spatially variable adsorption is perhaps the simplest explanation.

An analysis of the major element geochemistry of the fluids sampled at the springs, compensated for the input of Paradox brine, allowed Kampmann et al. (2009; their Eqn. 13) to describe the effects of the CO_2 input for the brine-affected zone by the following reaction:

plagioclase + K-feldspar + gypsum + dolomite + H^+ + HCO_3^- = kaolinite + smectite + calcite + quartz

It seems reasonable to assume that a similar reaction is occurring in the zone that lacks brine and free-phase CO_2, driven by CO_2 derived from the atmosphere and any soil processes. Hence, trace metals could be introduced into the aquifer waters by dissolution of any of plagioclase, K-feldspar, gypsum or dolomite. Given that the concentration of CO_2 associated with atmosphere and soil processes in a semi-arid environment will be much lower than associated with free-phase CO_2, then any trace metal input from the above reaction is likely to be much less prior to the input of high CO_2 concentrations than afterwards. Kampmann et al. (2009) corrected the major element concentrations in the spring waters for the input of the Paradox brine, however it is not possible to accurately correct the trace metal concentrations using the same method, as the only published analysis of the brine (Spangler, 1992) does not include the appropriate metals. It is possible to

calculate relative trends of element concentrations as these are independent of the Paradox brine composition – hence the graphs in Fig. 9 have no absolute concentration (y-axis) units and are only relative values. Comparing the data for As, Cu and Ni to the modelled reaction from Kampmann et al. (2009; Fig 9 lower right) is apparent that there is no correlation between the extent of the reaction and the concentrations of the trace metals for As or Ni, though Cu is more equivocal. From this it is concluded that the trace metals are not derived by the dissolution of feldspars, gypsum or dolomite (with the possible exception of Cu). Neither can they be derived by the dissolution of kaolinite, smectite, calcite or quartz as these are modelled as precipitating (Kampmann et al., 2009).

There is however evidence for the dissolution (and possibly precipitation) of an Fe-bearing phase that is not modelled by Kampmann et al. (2009). Concentrations of Fe vary greatly both between individual sampling locations and between different studies. The highest concentrations were reported by Kampman et al. (2014) at Champagne Geyser (14.9 mg/L) and for this study at Little Bubbling Spring (14.8 mg/L). These measured concentrations are similar to concentrations in leaching experiments using red sandstones from Utah, of up to 15 mg/L, using an H_2S-equivalent reducing agent (thioacetamide) with CO_2 (Purser et al., 2014). Using CO_2 with CH_4, a maximum of 3 mg/L Fe^{2+} was recorded, and < 1 mg/L with only CO_2 (Purser et al. 2014, their Figure 3), which is consistent with low concentrations obtained with the experiments for this study (maximum 0.2 mg/L; mode 0.009 mg/L; Table S1). By analogy with the experiments of Purser et al. (2014) the Fe is derived from Fe-rich grain coatings which are principally hematite. Experiments using the Mount Simon sandstone did find evidence for the dissolution of an iron-bearing phase (in this case pyrite; Dávila et al., 2020) but the study did not report trace metal concentrations. For the Green River springs, however, none of As, Cu or Ni correlate with Fe ($R^2 < 0.25$ in all cases), arguing against a simple dissolution / precipitation control for these elements. Wigley et al. (2012) speculated that trace metals are mobilised from Fe-oxide grain coatings but are re-deposited at a reaction front, limiting their overall mobility in the migrating fluids. Significant differences in Fe concentrations in individual springs between published studies may indicate changes in redox conditions in the N-aquifer with time, which can be explained as changes in the proportion of H_2S and / or methane to CO_2.

A test can be made for whether carbonate dissolution is contributing to concentrations of Ca, Mg and alkalinity in the Green River springs. A plot of Ca^{2+} and Mg^{2+} equivalent concentrations (meq/L) against HCO_3^- (meq/L), with a 1:1 relationship representative of a stoichiometric relationship between the cations and anion is indicative of carbonate dissolution (Stallard and Edmond, 1983). Fig. 10 shows the data for this study along with those obtained and calculated from the literature

(Heath et al. 2009; Kampman et al. 2009, 2014 and Shipton et al. 2004). The 1:1 stoichiometric relationship line is plotted for comparison. The data from Heath et al. (2009) and Shipton et al. (2004) clearly do not fit the 1:1 trend. The Kampman studies and this study's data both cluster around the 1:1 relationship and display a quasi-linear relationship. The conclusion therefore is that carbonate dissolution is occurring, however this is not the sole supply of Ca, Mg and HCO_3^- to the groundwaters. In contrast, Kampman et al. (2009) modelled the precipitation of calcite, but the dissolution of Ca-feldspars. Trace metal concentrations, where detected in the Green River springs, correlate poorly with major elements in most cases. While Pearson's correlation coefficients for a number of element pairs are indicative of strong relationships, further examination shows that these are often skewed by individual high or low values. Only Ca and Ni show a strong positive linear correlation. Nickel concentrations may therefore be related to carbonate dissolution.

The relatively high salinity of the springs (TDS from 3,750 to 17800 mg/L) exceeds the EPA secondary drinking water standard of 500 ppm by a factor of at least seven and in some cases a factor of over thirty. Hence, the spring waters are not deemed potable, and it could be argued that the remaining EPA drinking water standards cannot be meaningfully applied to these waters. However, the origin and controls of the trace metals may be applicable to CO_2-rich waters that are potable, and, in the unlikely event of a leak of engineered CO_2 into an underground supply of drinking water, it will be standards such as those of the EPA which will be used to determine what remediation is required. Trace metal concentrations in the CO_2-rich springs are significantly below legal limits for USA drinking water (except for As) despite previous reports of high trace metal loads in aquifers with high CO_2 contents (e.g. Little and Jackson, 2010). Overall, trace metal concentrations are low in water samples from 10 CO_2-rich springs and where present, their source or sources are uncertain. For As, this is plausibly introduced into the aquifer in solution in the Paradox brines, as above and hence may not be related directly to the high CO_2 concentrations.

Batch experiments

The batch experiments all used brine collected from Crystal Geyser as the initial aqueous fluid, therefore each experiment had 2 sources of trace metals, the brine and the rock samples. The results show that there was transfer of metals both from the rock to the brine, and the brine to the rock, discussed below.

Reactions prior to the addition of CO_2

For some metals, the concentrations recorded during the experiments are much lower than the pre-experiment porefluid concentrations (As < 0.02 vs 39 μg/L; Ni mostly < 0.04 vs 8 μg/L though

maximum values are comparable). Assuming that the metals were not lost to adsorption onto the vessels used for transport or the glass walls of the batch reaction vessels, then they must have been absorbed onto the surfaces of the rock grains. For As, the addition of CO_2 did not increase concentrations, but for Ni concentrations increased into the range observed in the spring waters, at least proving in this case that the low concentrations prior to CO_2 addition were not an artifact (Fig. 3).

For As, a potential explanation of the apparent adsorption of the metals and the very low (BDL) concentrations of As in the batch experiments even after the addition of CO_2 is that the rock samples used in the experiments have very low (mobile) As concentrations. The samples are from the San Raphael swell, i.e. the recharge area for the N-aquifer system and lie on the regional flow path before the input of the deep-sourced brines, and hence before the As input apparently associated with the Paradox brines (see above). Any mineral surfaces that are capable of adsorbing As will be 'undersaturated' with the metal as they have not been exposed to high concentrations, and hence will be capable of absorbing As from solution. Arsenic concentrations are very low (BDL) in the experiments since the As is not derived from the rock matrix, and is hence it is not present to be leached from the rocks during the experiments. The same argument cannot be made for Ni, as this is not added to the aquifers by the brines, as above, but must be derived from the rock matrix. It is possible that much of any previously adsorbed Ni in the San Rafael rock samples has been desorbed and removed by meteoric water leaching, leaving mineral surfaces available for adsorption. For other metals, the concentrations in the batch reactions exceed those in the initial fluid (Cr 0 - 3 vs < 0.3 μg/L; Zn 25 – 50 vs < 0.2 μg/L; Pb 0 – 5 vs < 0.035 μg/L). These metals must have been derived from the rock samples.

The concentration of Ca, Mn and Sr all declined in the pre-CO_2 phase of the experiments, from values at or close to the range of the springs, to values below this. This implies the precipitation of a Ca-bearing phase, and given that Mg does not follow the same trend, then the phase is presumably calcite rather than dolomite. This is associated with a pH change of approximately 7 to 9, which will cause the reaction of much of the HCO_3^- to CO_3^{2-}, which may have been caused by a gradual de-gassing of the Crystal Geyser water in the experiments prior to the introduction of the CO_2.

Reactions after the addition of CO_2

The addition of CO_2 to the experiments reversed the trends seen in Ca, Mn and Sr, implying that the newly precipitated calcite was at least partly re-dissolved (Fig. 4). With only a single exception (Mn for sample S4) the initial concentrations were not attained, so that the dissolution was not complete.

The dissolution was rapid (a few days at most), after which concentrations of Ca, Mn and Sr remained constant or increased only slowly. None of the trace elements show similar trends, so that neither the precipitation of calcite nor the subsequent dissolution appeared to have controlled trace element concentrations. Correlations between the 8 trace metals and Ca, Mg and Fe are either weak or non-existent, supporting the notion that carbonate dissolution and precipitation are not strong controls on the concentrations of trace metals in the batch experiment fluids.

A half of the trace elements (Cr, Cu, Pb and Zn) show relatively high concentrations in the days after the introduction of the CO_2, but in all cases decline to values similar (Pb) or lower (Cr, Cu, Zn) than before the addition of CO_2. The trace metals with temporary increased concentrations upon addition of CO_2 were generally those which have an association with carbonates (Cu, Pb and Zn but not Ni), but this may be coincidence, as above. It may be significant that the transient spikes in concentration coincide with a period of anomalously low pH (Fig. 11), which was subsequently buffered back to the range of values recorded within the natural springs. A pH control on absorption / desorption on mineral surfaces is therefore possible (e.g. Hsia et al., 1994). These transient spikes in concentration would have little or no effect upon a natural system, where water flow rates might transport dissolved metals for distances that would be very small compared to the dimensions of the natural aquifer system.

The only trace elements that show convincing and sustained increases in concentration upon addition of CO_2 are Ni and Pb (Fig. 3). Nickel is commonly cited in the literature as being enhanced with the addition of CO_2 to batch experiments with calcareous sandstones and sands, similar to the samples used in this study (Little and Jackson, 2010; Lu et al., 2010 and Cahill et al., 2013). However, the gradual increase in Ni does not correlate with the sudden increase in Ca after CO_2 addition – though this may be the re-dissolution of (low Ni) calcite precipitated in the pre-CO_2 stage of the experiments. It is notable that Ca does increase slowly for the remainder of the experiments after the sudden increase associated with the addition of CO_2. It is possible that this slower dissolution is liberating Ni, though not from the neo-formed (pre-CO_2) calcite but from pre-existing (authigenic) calcite. Similar arguments apply to Pb, which is also recorded as associated with carbonate mineral dissolution (e.g. Wilkinson et al., 2020). Lead also occurs in K-feldspars (Smith and Brown, 1988), and there is a steady increase in K after the addition of CO_2 which could indicate K-feldspar dissolution. Unlike the example reported by Wilkinson et al. (2020), where unfeasible concentrations of Pb would have been required in the feldspar to account for the observed solution compositions, here the calculated Pb concentrations are on the low side of the range expected (10–1000 ppm; Smith and Brown, 1988). Hence, the dissolution of K-feldspar is a plausible source of the Pb seen in the

experiments after the addition of the CO_2, and there is no significant correlation between Pb and pH (Fig. 11) so that desorption from mineral surfaces seems relatively unlikely.

Whereas Cd and Cr were found to be somewhat mobile with CO_2 in previous studies (Terzi et al., 2014), their mobility in this study was low, especially after the addition of CO_2 for Cr. Mercury responded initially to the CO_2 bubbling with increased concentrations, particularly for Entrada S2, but within days had returned back to BDL. The effect of CO_2 for Hg appeared therefore to be a temporary mobilisation, but which was not sustained beyond a few days, possibly due to volatilisation, i.e. loss from the reaction vessel. Alternatively, as Hg concentrations are high when pH is less than approximately 7 (Fig. 11) this could be interpreted as evidence for pH-dependant absorption / desorption, as above.

Concentrations of Fe in the experiments are low (0.005 - 0.177 mg/L) compared with concentrations found in the spring waters (1.2 - 14.8 mg/L). Iron mobility is low where it is oxidised to Fe^{3+}. Concentrations of Fe are higher in the spring waters most likely due to reducing conditions caused by dissolved methane (Wigley et al., 2013) or hydrogen sulphide (e.g., Purser et al. 2014). Purser et al. (2014) demonstrated that significant Fe^{2+} (3 - 15 mg/L) could be leached from Utah sandstone collected in the same area, using these reducing agents.

Conclusions

The concentrations of trace metals are low in the Utah spring waters (except for As) despite the presence of free-phase CO_2. All the waters (except for As and a single exception for Hg) meet USA EPA standards for drinking water except for total salinity which is largely derived from externally sourced (Paradox Formation) brine. Concentrations of 4 of the trace metals (Cd, Cr, Hg, Pb) are consistently below analytical detection limits. This shows that CO_2 in aquifers does not inevitably cause trace metal contamination.

The detectable trace elements in the spring waters are largely from brines sourced from the underlying Paradox Formation (As, Cu) or the rock matrix (Ni). For As, the experiments mobilised very little of the metal as it is not sourced from the rock, which may in fact be capable of absorbing (and hence immobilising) As. For Ni, the dissolution of carbonate minerals is a possible source, though the experiments show that pH-dependant adsorption is also a potential control. None of the trace metals perfectly fit a simple mixing model between Paradox brine and aquifer recharge, suggesting either that the Paradox brine is of variable composition, or that some of the trace elements (especially As) are adsorbed onto mineral surfaces within the aquifer.

With the exception of Fe, Pb and As, the concentration of trace metals in batch experiments are within the range, or close to, the concentrations found in the springs. Fe is probably affected by the oxidation state of the fluids in the experiments, rendering it comparatively insoluble compared to the subsurface brines. The addition of CO_2 to batch experiments reduces experimental pH values to just within the range of values for the springs in the Green River area, indicating the capacity of the rock to buffer pH.

Trace metal concentrations do not correlate well with any of the major elements including Ca, Mg and Fe (for carbonates). Therefore, where present, trace metal concentrations in the batch experiments are unlikely to be due to mineral dissolution (with the possible exception of Ni and more certain exception of Pb), and more likely the result of ion exchange / desorption processes, most plausibly involving Fe-oxide grain coatings.

Acknowledgements

Sampling kits for the spring waters were provided by Dr. Pat Mickler and Dr. Staci Loewy of the Jackson School of Geosciences, University of Texas (UT). KC was co-funded by the UK EPSRC and ScottishPower. Neither organisation was involved in the design or interpretation of the work.

References

Cahill, A. G., Jakobsen, R., Mathiesen, T. B., and Jensen, C. K., 2013, Risks attributable to water quality changes in shallow potable aquifers from geological carbon sequestration leakage into sediments of variable carbonate content. International Journal of Greenhouse Gas Control, 19, 117–125.

Dávila, G., Dalton, L., Crandall, D.M., Garing, C., Werth, J.W., Druhan, J.L., 2020, Reactive alteration of a Mt. Simon Sandstone due to CO_2-rich brine displacement. Geochimica et Cosmochimica Acta, 271, 227-247.

Environmental Protection Agency 2022A. National Primary Drinking Water Regulations, https://www.epa.gov/ground-water-and-drinking-water/national-primary-drinking-water-regulations

Environmental Protection Agency 2022B. Secondary Drinking Water Standards: Guidance for Nuisance Chemicals, https://www.epa.gov/sdwa/secondary-drinking-water-standards-guidance-nuisance-chemicals

Han, W.S., Watson, Z.T., Kampman, N., Grundl, T., Graham, J.P., Keating, E.H., 2017, Periodic changes in effluent chemistry at cold-water geyser: Crystal geyser in Utah. Journal of Hydrology, 550, 54–64.

Hanshaw, B.B., Hill, G.A., 1969. Geochemistry and hydrodynamics of the Paradox basin region, Utah, Colorado and New Mexico. Chemical Geology, 4, 263–294.

Haszeldine, R.S., Quinn, O., England, G., Wilkinson, M., Shipton, Z.K., Evans, J.P., Heath, J., Crossey, L., Ballentine, C.J. and Graham, C.M., 2005. Natural geochemical analogues for carbon dioxide storage in deep geological porous reservoirs, a United Kingdom perspective. Oil & gas science and technology, 60, pp.33-49.

Heath, J. E., Lachmar, T. E., Evans, J. P., Kolesar, P. T., and Williams, A. P. (2009). Hydrogeochemical characterization of leaking, carbon dioxide-charged fault zones in east-central Utah, with implications for geologic carbon storage. Geophysical Monograph Series, 183:147–158.

Hsia, T.-H., Lo, S.-L., Lin, C.-F., Lee, D.-Y., 1994. Characterization of arsenate adsorption on hydrous iron oxide using chemical and physical methods. Colloid. Surface. Physicochem. Eng. Aspect. 85, 1–7.

Kampman, N., Bickle, M., Becker, J., Assayag, N., and Chapman, H. (2009). Feldspar dissolution kinetics and Gibbs free energy dependence in a CO_2-enriched groundwater system, Green River, Utah. Earth and Planetary Science Letters, 284(3-4):473–488.

Kampman, N., Bickle, M., Maskell, A., Chapman, H., Evans, J., Purser, G., Zhou, Z., Schaller, M., Gattacceca, J., Bertier, P., Chen, F., Turchyn, A., Assayag, N., Rochelle, C., Ballentine, C., and Busch, A. (2014). Drilling and sampling a natural CO_2 reservoir: Implications for fluid flow and CO_2-fluid–rock reactions during CO_2 migration through the overburden. Chemical Geology, 369:51–82.

Kampman, N., Burnside, N. M., Shipton, Z. K., Chapman, H. J., Nicholl, J. A., Ellam, R. M., and Bickle, M. J. (2012). Pulses of carbon dioxide emissions from intracrustal faults following climatic warming. Nature Geoscience, 5(5):352–358.

Kharaka, Y. and Hanor, J. (2007). Deep fluids in the continents: 1. Sedimentary basins. In Drever, J., editor, Surface and Ground Water, Weathering and Soils. Treatise on Geochemistry 5. Elsevier, San Diego.

Little, M. G.; Jackson, R. B., 2010, Potential Impacts of Leakage from deep CO_2 Geosequestration on Overlying Freshwater Aquifers. Environ. Sci. Technol. 44, 9225 – 9232

Lu, J., Partin, J. W., Hovorka, S. D., and Wong, C. (2010). Potential risks to freshwater resources as a result of leakage from CO_2 geological storage: a batch-reaction experiment. Environmental Earth Sciences, 60(2):335–348.

Purser, G., Rochelle, C., Rushton, J., Pearce, J., and Wagner., D. (2014). An experimental and analogue study of iron release from red sandstones. Energy Procedia, 63:3268–3274.

Shipton, Z. K., Evans, J. P., Kirschner, D., Kolesar, P. T., Williams, A. P., and Heath, J. (2004). Analysis of CO_2 leakage through 'low-permeability' faults from natural reservoirs in the Colorado Plateau, east-central Utah. Geological Society, London, Special Publications, 233(1):43–58.

Smith, J.V., Brown, W.L., 1988. Feldspar Minerals, Volume 1, Crystal Structures, Physical, Chemical and Microtextural Properties. Springer-Verlag, Berlin.

Spangler, L. E. (1992). Records of wells in sandstone and alluvial aquifers and chemical data for water from selected wells in the Navajo aquifer in the vicinity of the Greater Aneth Oil Field, San Juan County, Utah. Technical report, U.S. Geological Survey.

Stallard, R. and Edmond, J. (1983). Geochemistry of the Amazon 2. The influence of geology and weathering environment on the dissolved load. Journal of Geophysical Research, 88(C14):9671–9688.

Terzi, K., Aggelopoulos, C. a., Bountas, I., and Tsakiroglou, C. D. (2014). Effects of carbon dioxide on the mobilization of metals from aquifers. Environmental Science and Technology, 48:4386–4394.

Wigley, M., Kampman, N., Chapman, H. J., Dubacq, B., and Bickle, M. J. (2013). In situ redeposition of trace metals mobilized by CO_2-charged brines. Geochemistry, Geophysics, Geosystems, 14(5):1321–1332.

Wigley, M., Kampman, N., Dubacq, B., and Bickle, M. (2012). Fluid-mineral reactions and trace metal mobilization in an exhumed natural CO_2 reservoir, Green River, Utah. Geology, 40(6):555–558.

Wilkinson, M., Gilfillan, S.M., Haszeldine, R.S. and Ballentine, C.J., 2009. Plumbing the depths: Testing natural tracers of subsurface CO_2 origin and migration, Utah. In : Carbon Dioxide Sequestration in Geological Media—State of the Science. Eds(s) M. Grobe; J. C. Pashin; R. L. Dodge American Association Petroleum geologists Studies in Geology 57. https://doi.org/10.1306/13171266St591353

Wilkinson, M., Carruthers, K., Thomas, A.L., and Haszeldine, R.S., 2020, The performance of leaching experiments to assess the potential mobilization of trace elements during CO_2 injection. Applied Geochemistry, 120, 104667.

Figure Captions

Fig. 1. Location map of outcrop and spring water sampling areas in the San Rafael Desert, near Green River, Utah. Clustered samples are expanded for clarity, top left and bottom left for outcrop rock samples and spring samples, respectively.

Fig. 2. pH values for the batch reactions. CO_2 flow commences at day 82. Shaded area indicates the field-measured pH values of the Green River spring waters.

Fig. 3. Concentrations of trace metals for the batch experiments. Dashed vertical line at day 82 represents start of CO_2 flow. Shaded areas indicate the range of concentrations detected across 10 Green River spring locations (Figure 1). No shading present indicates element concentrations fall below analytical detection limits.

Fig. 4. Concentrations of elected major elements for the batch experiments. Dashed vertical line at day 82 represents start of CO_2 flow. Shaded areas indicate the range of concentrations detected across 10 Green River spring locations (Figure 1). No shading present indicates element concentrations fall below analytical detection limits, except Fe where the springs' range is significantly greater than the batch concentrations.

Fig. 5. Chloride concentration versus distance from the airport well.

Fig. 6. Arsenic and Cu concentrations for the Airport Well (dark circles) are low compared to the other springs, but Ni lies within the range of the other spring water analyses.

Fig 7. Concentrations of As vs Cl for the spring waters. See text for interpretation.

Fig. 8. Concentrations of Cu vs Cl for the spring waters. See text for interpretation.

Fig. 9. Trace element concentrations in the N-aquifer versus distance from the Airport Well show no similarity to the modelled dissolution of K-feldspar modelled by Kampmann et al., 2009) for As or Ni, though some resemblance for Cu. The plotted concentrations are corrected for the input of Ismay brine using the method of Kampmann et al. (2009) and are relative values as the trace metal concentrations in the brine are unknown. The lower right figure shows calculated changes in feldspar abundance versus distance from the Airport Well, redrawn from Kampman et al. (2009).

Fig. 10. Spring water analyses plot close to a 1:1 line for carbonate vs Ca plus Mg in this study and those of Kampmann (2009, 2014), supporting carbonate mineral dissolution as a source of alkalinity.

Fig 11. Scatter plot of pH and Utah batch concentration data. Arsenic not shown as concentrations all BDL. Error bars are 2σ of the mean of standard reference materials.

Table Captions

Table 1. Concentration limits in USA drinking water, EPA National Primary Drinking Water Regulations

Table 2. Rock sample details

Table 3 Spring sampling bottle types, volumes, type of subsequent analysis, and chemical additives. *Volatile Organic Analysis vial.

Table 4. Field measurements of spring waters.

Table 5. Spring water composition by ICP-MS. *Concentrations in mg/L. **Hg analysed by ICP-MS at University of Edinburgh. Blank concentration values are < LOD, or not reported.

Table 6. Composition of the rock samples by XRD.

	MCLG[1] (mg/L)	MCL[2] (mg/L)
As	0	0.01
Cd	0.005	0.005
Cr	0.1	0.1
Cu	1.3	1.3
Hg (inorganic)	0.002	0.002
Ni	Not regulated	Not regulated
Pb	0	0.015
Zn	Not regulated	5 (secondary MCL)

[1] Maximum Contaminant Level Goal (MCLG) [2] Maximum Contaminant Level (MCL)

Source: Environmental Protection Agency (2020A, B)

Table 1

Sample	Latitude	Longitude	Formation	Description	Mass of sample / g
S1	38.9217500	-110.4300278	Entrada	Upper portion: mottled red/dark pink and white, medium grained, massive. Lower portion: Mottled white/pale cream and pink, fine grained, subrounded, well sorted, with occasional small (< 1 mm) dark feldspars. Friable surface, otherwise well cemented (calcite)	29.80
S2	38.9217500	-110.4300278	Entrada	Red, well sorted, well cemented (calcite), massive	29.60
S3	38.9230547	-110.4437193	Wingate	Pink/light red on surface crust, white underneath crust, fine-medium, well sorted with mm-scale cross-bedding. Friable.	31.00
S4	38.9224444	-110.4404722	Navajo	Pink and white, fine-medium, well sorted, friable with mm-scale cross bedding and 1 - 2 mm dark flecks throughout.	30.10

Table 2

Container	Volume (mL)	Analysis Type	Additives
Amber glass VOA*	40	Alkalinity	-
Amber glass VOA	40	Mercury	2% v/v 1M $K_2Cr_2O_7$ + 2% v/v 1N H_2SO_4
Amber glass VOA	20	Dissolved Inorganic Carbon	-
Polypropylene bottle	30	Trace elements	2% v/v 7N HNO_3
Polypropylene bottle	30	Major cations & anions	-
Polypropylene bottle	60	Archive	2% v/v 7N HNO_3

Table 3

Location	**pH**	**Alkalinity as HCO_3^- mg/L**	**Temperature / °C**
Green River Airport Well	6.31	2,334	26.6
Crystal Geyser	6.71	4,419	17.3
Big Bubbling Spring	6.65	4,148	15.6
Little Bubbling Spring	6.49	4,539	15.3
Side Seep	6.61	-	22.3
Tenmile geyser	6.34	3,589	16.5
Pseudo-Tenmile Geyser	6.56	3,820	17.4
Torrey's Spring	6.67	4,837	16.2
Tumbleweed Geyser	6.63	4,166	18.5
Champagne Geyser / Chaffin Ranch	6.80	3,616	13.8

Table 4

		Green River Airport Well		Crystal Geyser		Little Bubbling Spring		Big Bubbling Spring		Side Seep		Tenmile Geyser		Pseudo-Tenmile Geyser		Torrey's Spring		Tumbleweed Geyser		Chaffin Ranch Geyser	
	LoD	**Spring water composition by ICP-MS**																			
	mg/L	mg/L	±	mg/L	±	mg/L	±	mg/L	±	mg/L	±	mg/L	±	mg/L	±	mg/L	±	mg/L	±	mg/L	±
Al	0.183	-	-	-	-	-	-	-	-	-	-	-	-	-	-	-	-	-	-	-	-
As	0.021	8.63	0.62	38.9	7.1	38.3	5.5	55.4	7.4	-	-	13.3	2.4	59.8	7	56.2	11.2	17.5	2.6	6.59	2.13
Ba	0.034	16.2	0.5	14.3	0.9	13.9	0.5	8.96	0.51	34.4	0.8	13.9	0.9	8.79	0.84	9.57	0.58	9.65	0.77	6.21	0.48
Ca*	0.011	781	4	1,019	5	1,035	13	870	6	541	0	900	9	790	2	939	6	856	2	1,060	6
Cd	0.03	-	-	-	-	-	-	-	-	-	-	-	-	-	-	-	-	-	-	-	-
Cr	0.279	-	-	-	-	-	-	-	-	-	-	-	-	-	-	-	-	-	-	-	-
Cu	-0.07	-	-	13.5	2.8	36.5	0.7	24.5	1.6	21.2	1.2	31.3	0.9	26.2	0.9	40	3.1	24.4	1.4	25.6	2
Fe	0.111	4,856	51	11,638	176	14,817	202	6,707	113	1,190	14	3,763	58	4,817	99	7,382	100	3,753	39	3,351	49
Hg**	0.018	-	-	-	-	-	-	-	-	-	-	-	-	-	-	-	-	-	-	-	-
K*	0.006	92	2	308	4	312	6	390	3	411	9	259	5	393	5	453	10	336	5	303	6
Li	0.245	119	1	2,916	29	3,635	12	4,904	37	4,986	6	3,545	45	5,127	33	5,469	51	4,191	52	4,260	52
Mg*	0.004	186	2	226	1	230	1	214	1	222	1	233	1	200	1	192	0	212	1	237	1
Mn	0.145	1,216	2	1,634	9	1,135	3	416	4	355	2	1,052	9	120	1	1,069	6	943	8	935	2
Nay	0.042	495	2	3,570	14	3,831	33	5,484	31	5,690	23	5,598	15	5,811	28	6,234	181	4,807	21	4,916	44
Ni	0.041	7.41	0.28	8.13	0.62	11.6	1.5	7.43	0.97	4.36	0.55	8.96	1.27	6.36	0.72	8.24	0.74	8.61	0.85	11.7	0.9
Pb	0.035	-	-	-	-	-	-	-	-	-	-	-	-	-	-	-	-	-	-	-	-
Si	4.52	31,556	2,648	6,877	676	5,127	357	4,551	367	4,253	415	4,558	508	4,215	238	4,076	415	4,381	395	3,910	319
Sr	0.313	9,748	9	14,756	100	15,715	143	14,004	38	8,364	12	20,429	116	14,532	129	12,929	125	13,552	53	14,341	110
Zn	0.192	6.66	0.26	-	-	30.2	1.4	-	-	-	-	15.4	9.9	-	-	-	-	37	7.1	-	-
Spring water composition by ion chromatography analyses																					
Ca^{2+}		820	1	1,034	1	1,050	1	912	1	596	1	939	1	821	1	998	1	907	1	558	1
K^{+}		91	0.1	303	0.2	317	0.2	385	0.3	383	0.3	261	0.2	389	0.3	450	0.3	336	0.3	298	0.2
Li^{+}		-	-	3	0	4	0	5	0	5	0	3	0	5	0	6	0	4	0	4	0
Mg^{2+}		197	2	236	2	233	2	217	2	230	2	236	2	204	2	202	2	221	2	244	2
Na^{+}		458	1	3,272	5	3,887	5	5,076	7	5,367	7	5,203	7	5,372	7	5,971	8	4,447	6	4,584	6

NH_4^+		-	-	-	-	-	-	-	-	-	-	-	-	-	-	-	-	-	-	-
Br^-		-	-	2.15	0.01	2.03	0.01	3.9	0.02	3.22	0.01	5.89	0.02	2.93	0.01	3.88	0.02	2.75	0.01	2.61	0
Cl^-		115	0.4	3,966	15	4,777	18	6,122	23	6,432	24	7,085	27	6,352	24	6,975	26	5,334	20	5,676	21
F^-		-	-	-	-	-	-	-	-	-	-	-	-	-	-	-	-	-	-	-	-
NO_2^-		-	-	-	-	-	-	-	-	-	-	-	-	-	-	-	-	-	-	-	-

Table 5

Mineral	Entrada S1	SE	Entrada S2	SE	Wingate S3	SE	Navajo S4	SE	Navajo S5	SE
Gypsum	0.4	0.1	0.4	0.1	0.4	0.2	0.3	0.1	0.3	0.1
Ankerite	2.5	0.3	3.7	0.4	0.3	0.4	0.1	0.2	-	-
Calcite	5.1	0.2	4.7	0.3	0.3	0.1	0.7	0.1	0.07	0.08
Dolomite	5.4	0.3	3.3	0.5	-	-	0.2	0.1	0.1	0.3
Siderite	0.01	0.06	-	-	0.2	0.1	0.01	0.05	-	-
Hematite	0.2	0.1	0.3	0.1	0.2	0.1	0.3	0	0.3	0.1
Pyrite	0.12	0.05	-	-	0.01	0.06	0.13	0.05	0.08	0.05
Albite	6.1	0.4	3.4	0.3	1.2	0.3	0.5	0.2	0.5	0.3
Anorthite	1.8	0.4	1.2	0.4	0.1	0.3	0.4	0.3	0.3	0.3
Chlorite	1.9	0.6	1.1	0.4	1.3	0.4	0.7	0.3	0.8	0.3
Illite	6.6	0.4	2.6	0.6	2.1	0.3	1.6	0.3	1	0.3
Kaolinite	0.8	0.2	0.4	0.2	1.9	0.3	0.4	0.2	0.3	0.2
Microcline	4	0.3	4.8	0.4	5.9	0.5	5.3	0.4	3.6	0.4
Muscovite	4.1	0.4	1.2	0.4	2.1	0.3	1.4	0.3	1.1	0.3
Orthoclase	4.4	0.3	4.6	0.4	3.4	0.3	3.9	0.3	1.6	0.3
Quartz	56.7	1	68.3	0.1	80.7	1.1	84.2	0.9	89.7	0.9

Table 6

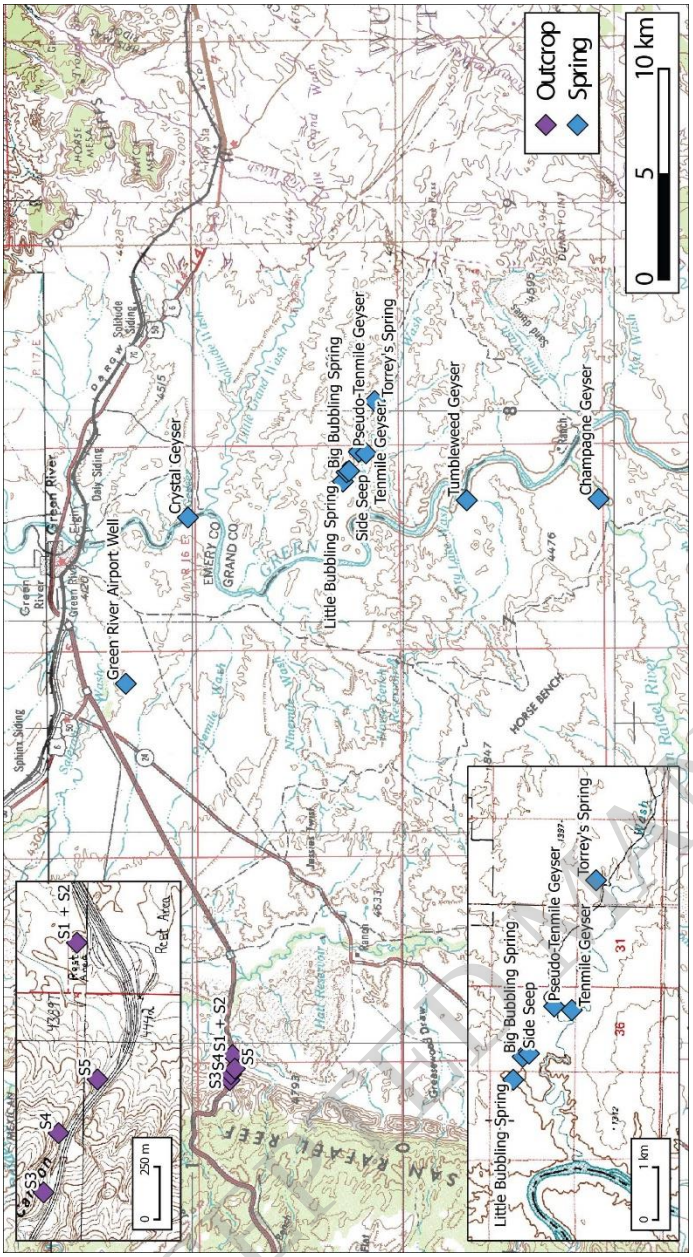

Figure 1

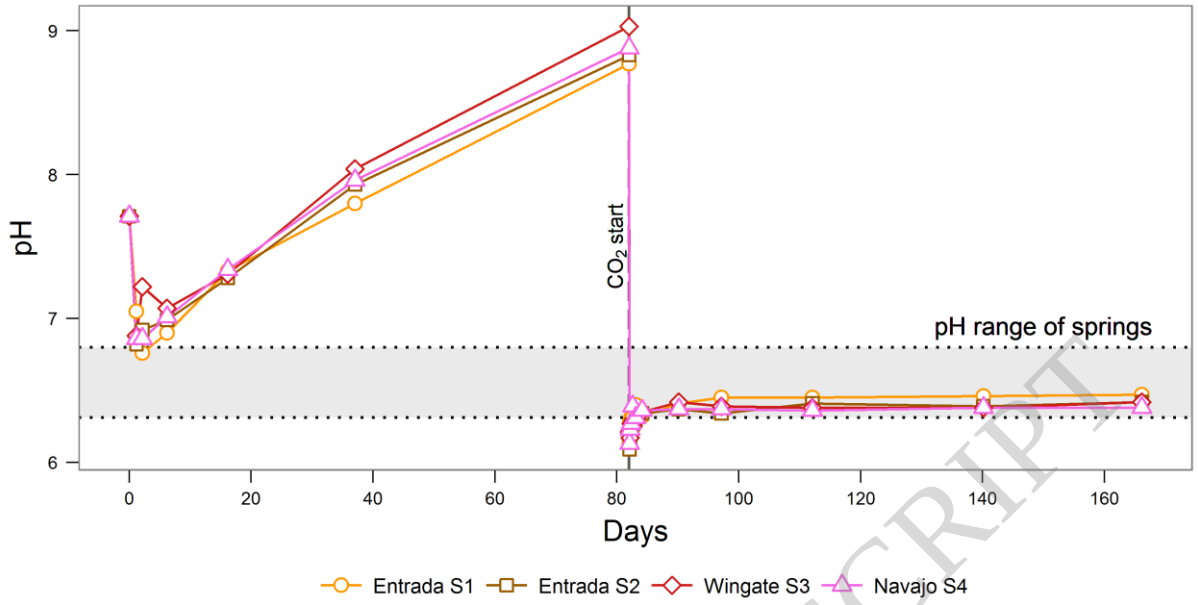

Figure 2

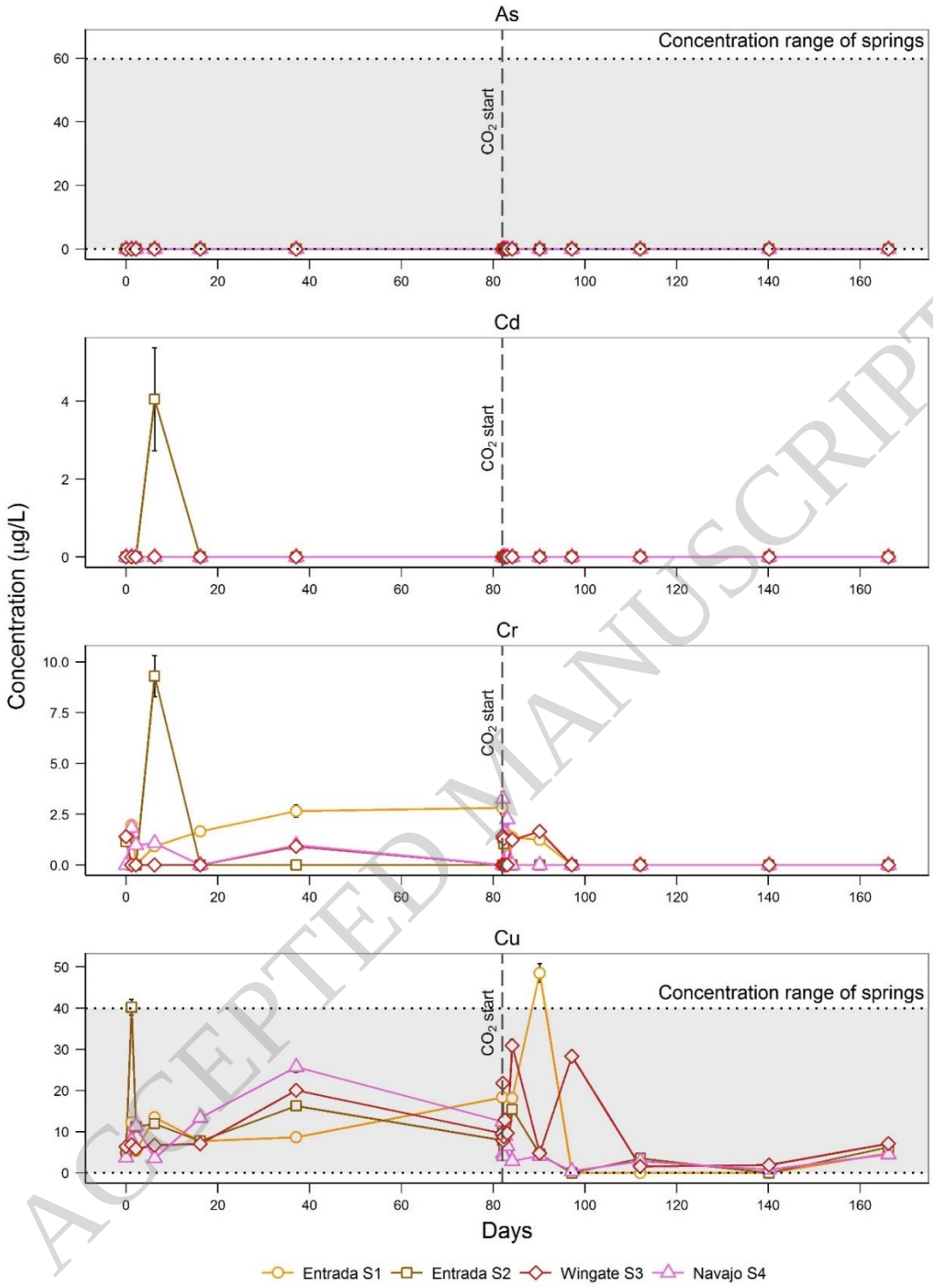

Figure 3

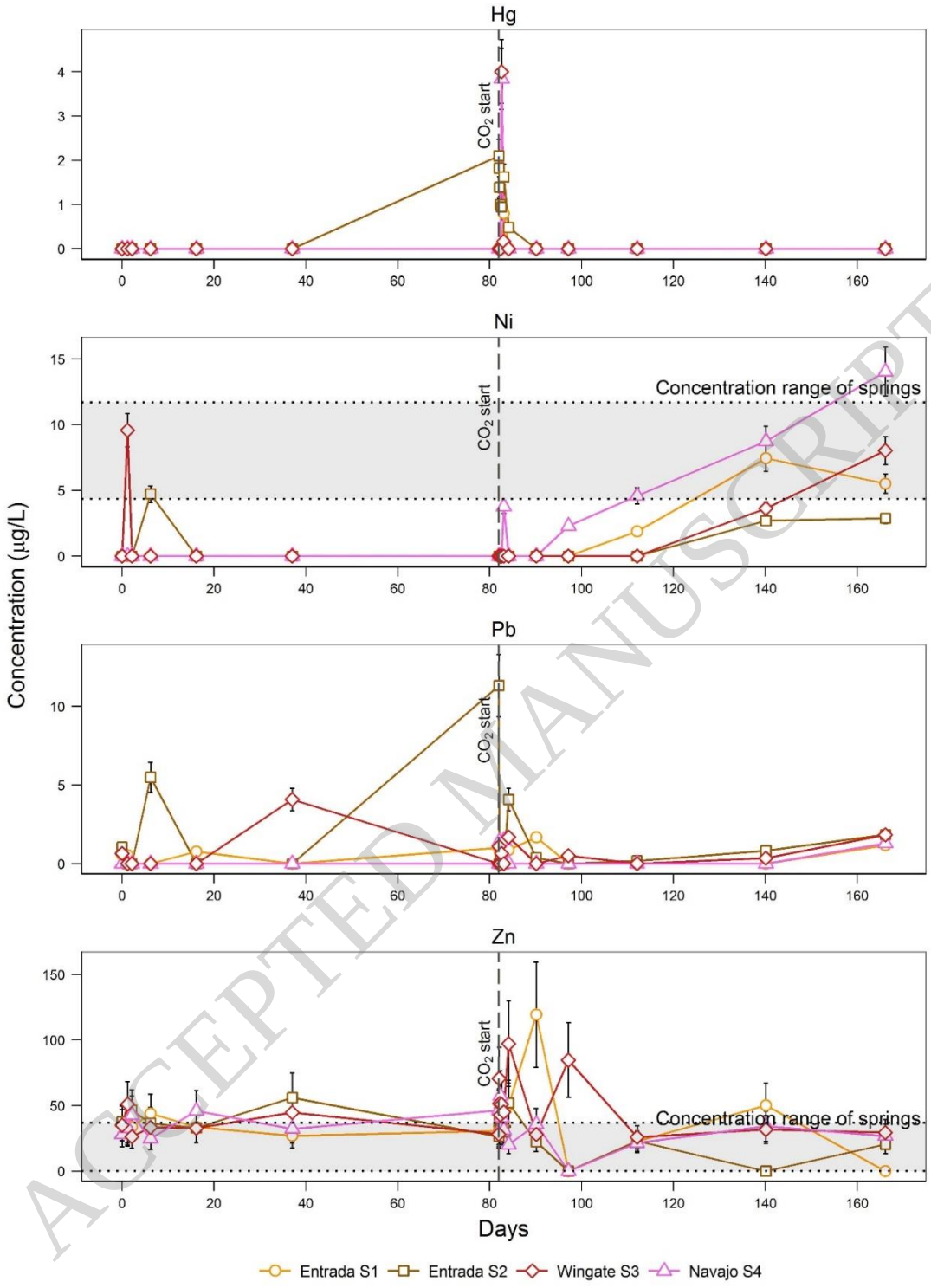

Figure 3(continued)

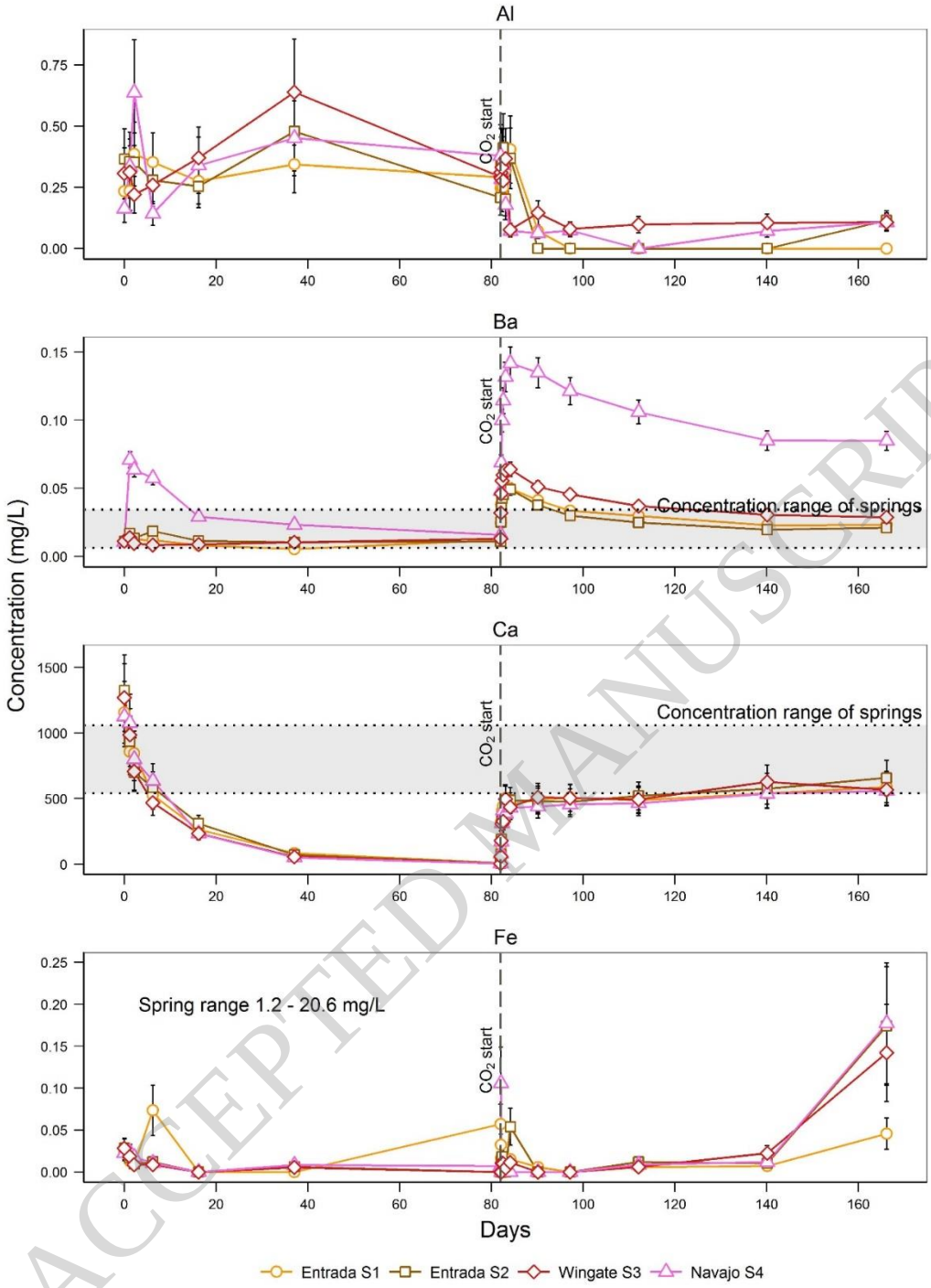

Figure 4

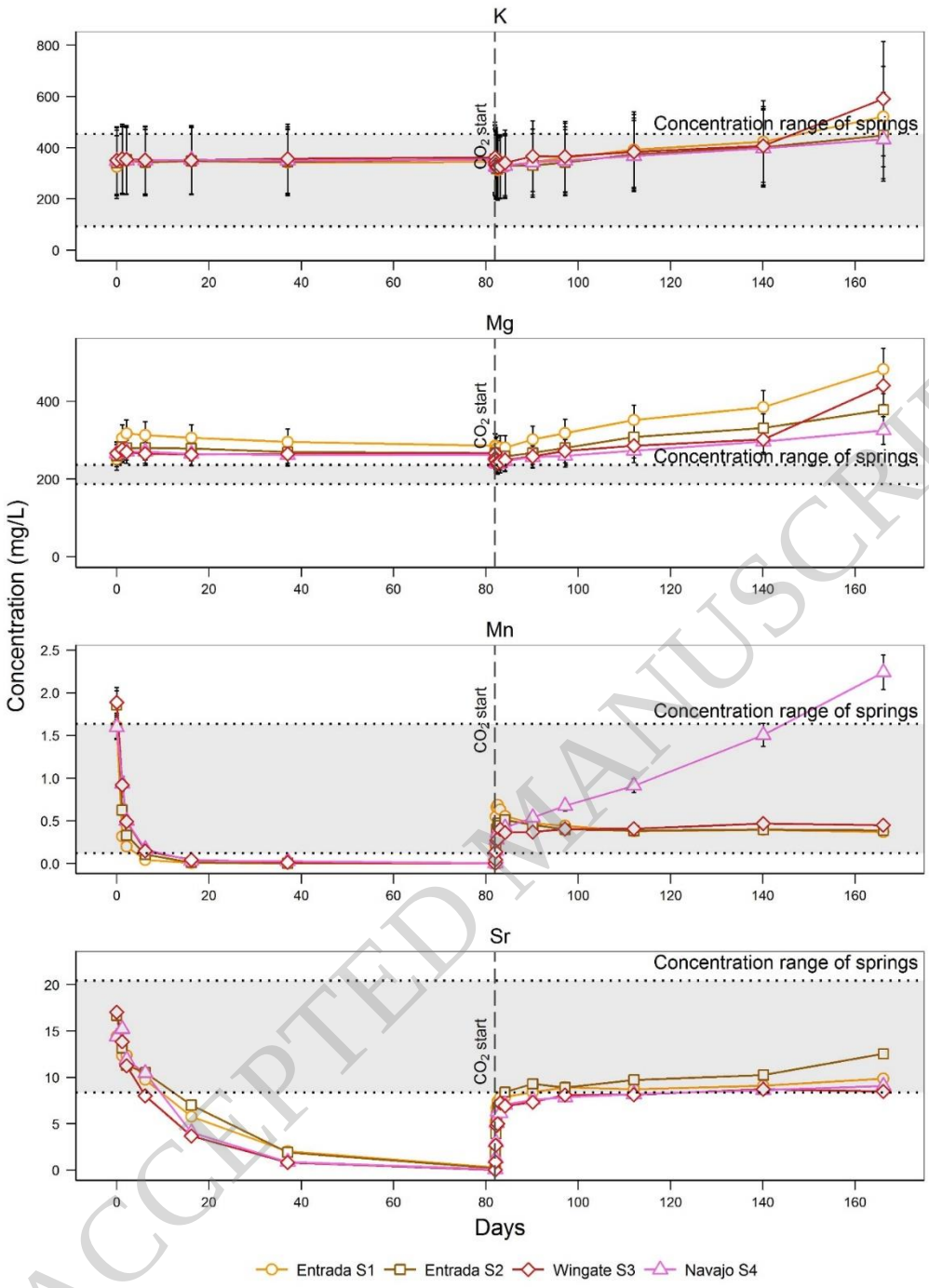

Figure 4(continued)

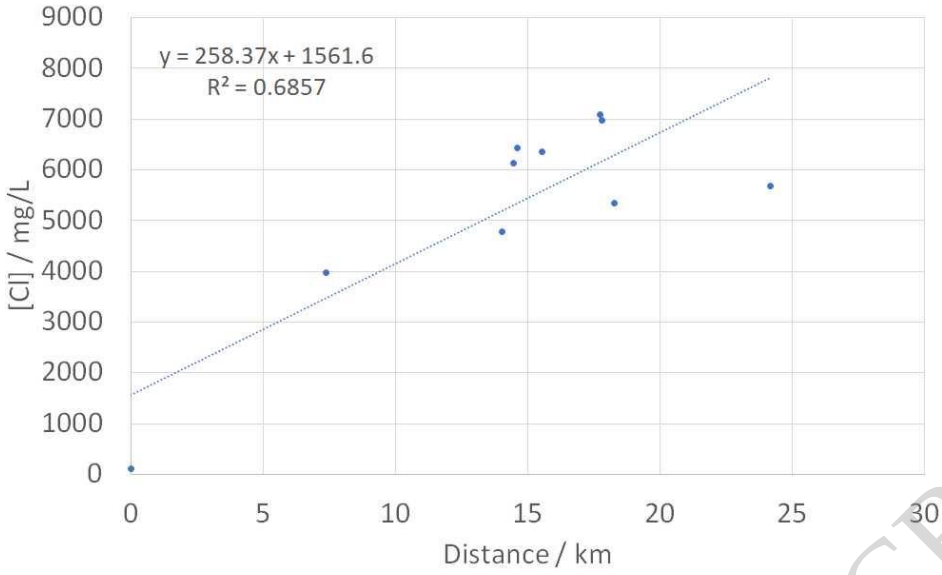

Figure 5

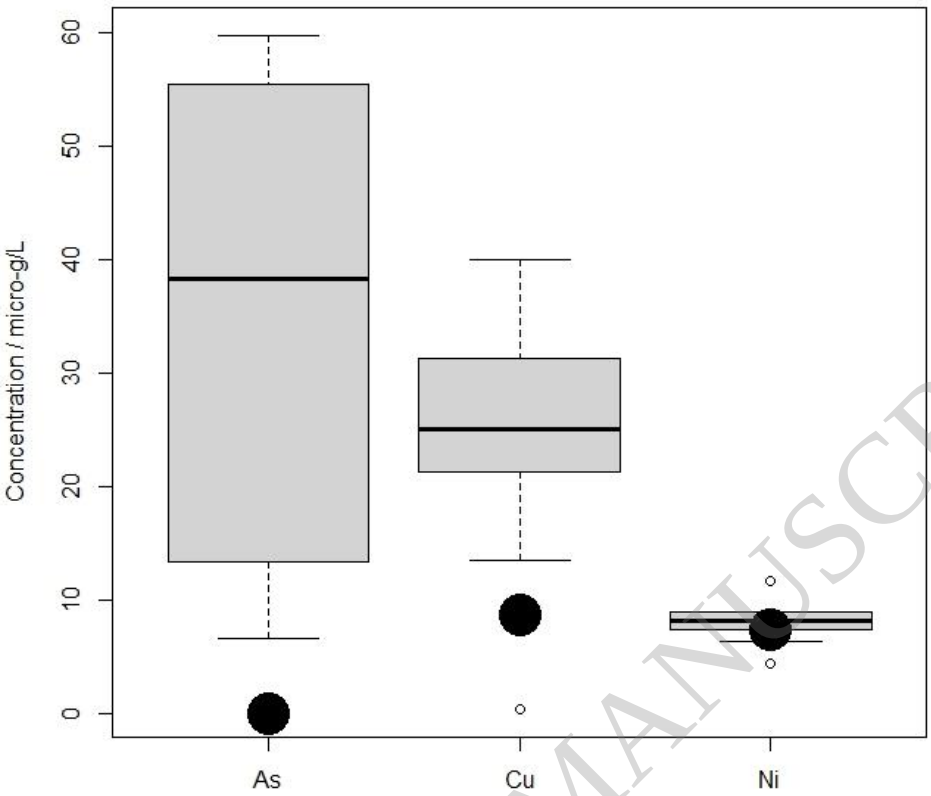

Figure 6

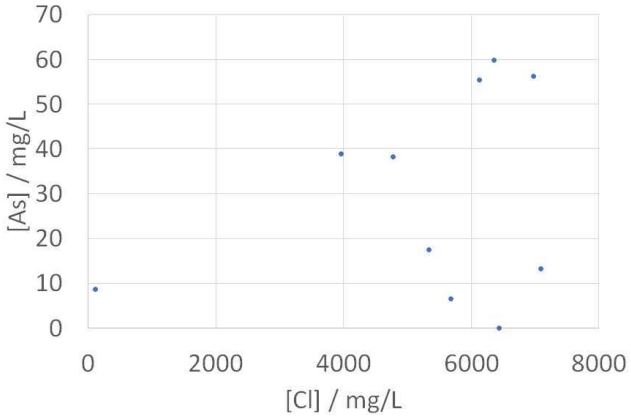

Figure 7

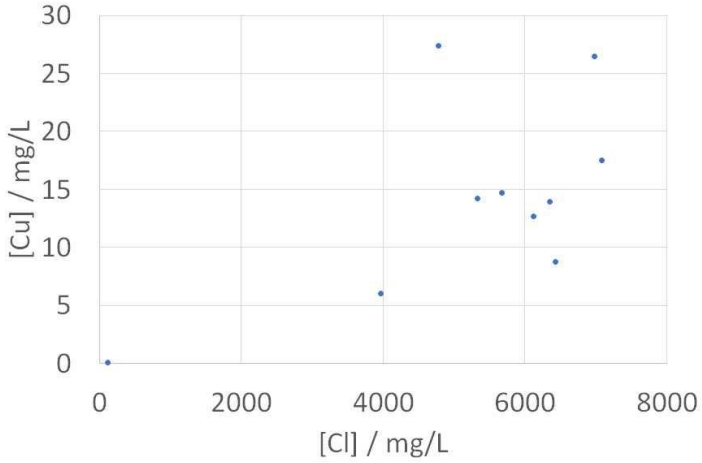

Figure 8

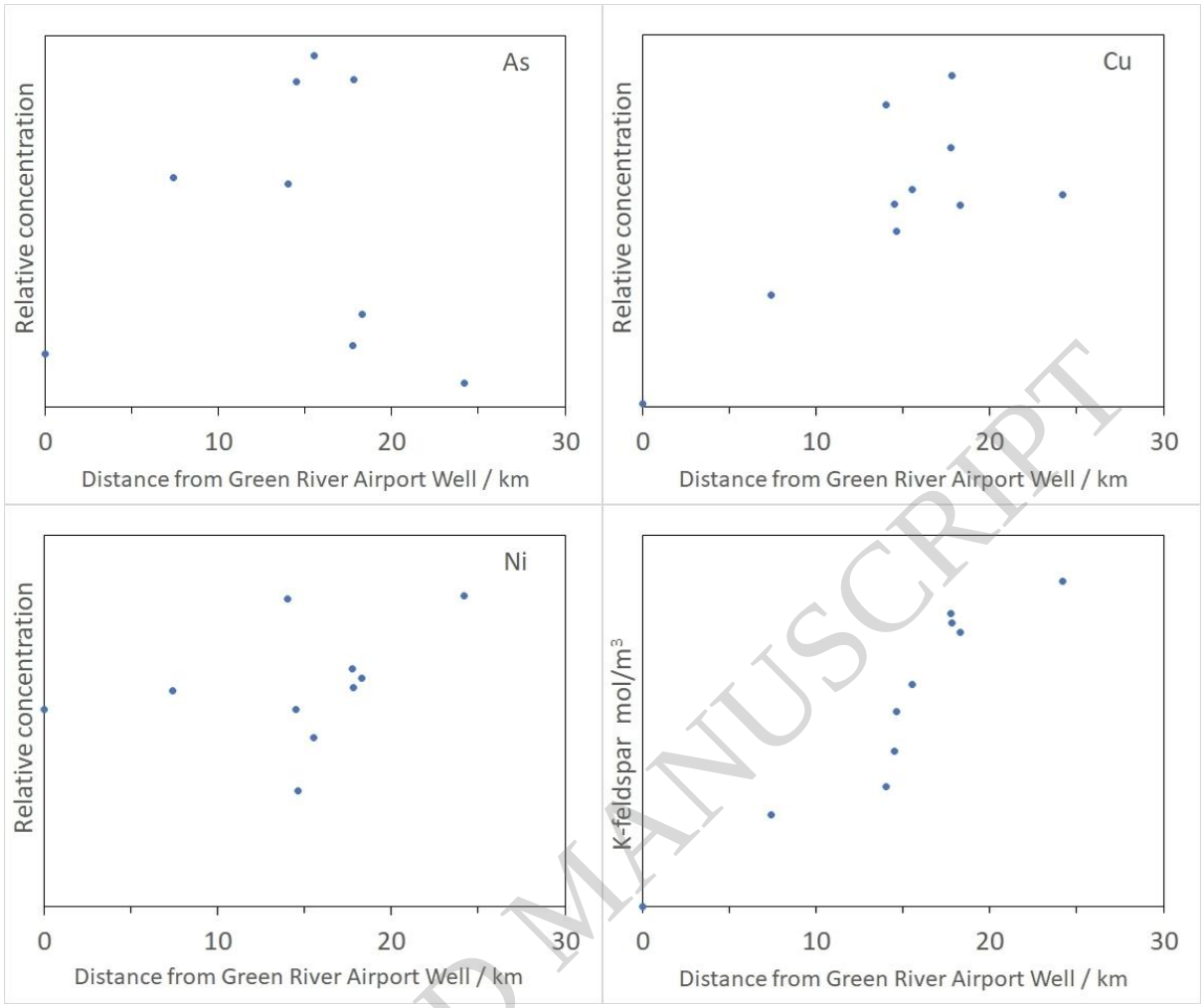

Figure 9

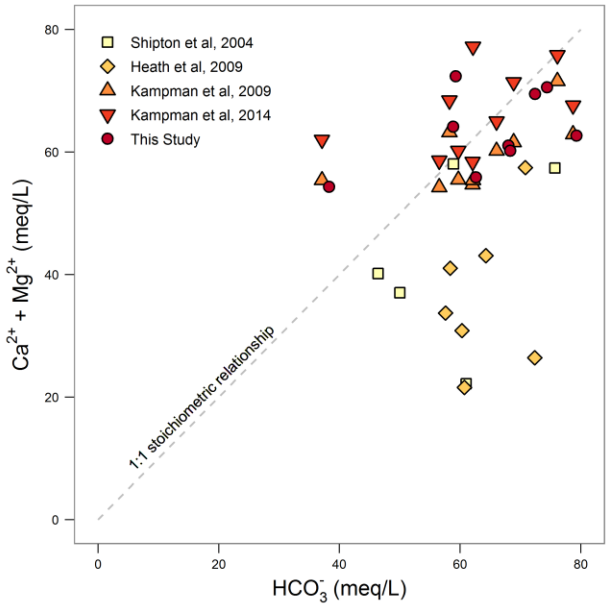

Figure 10

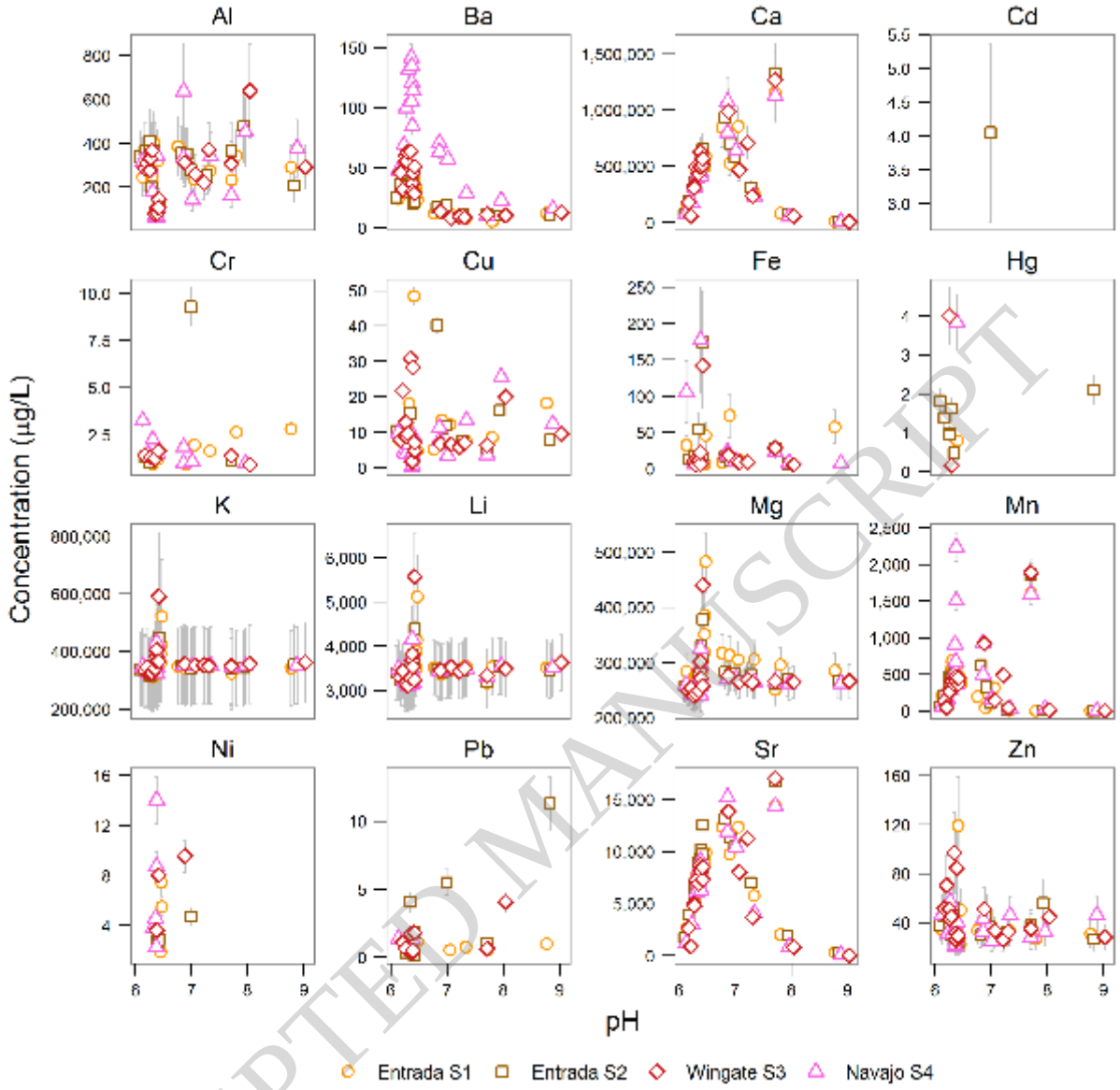

Figure 11